



HAL
open science

High-temperature measurements of acetylene VUV absorption cross sections and application to warm exoplanet atmospheres

Benjamin Fleury, Mathilde Poveda, Yves Benilan, Roméo Veillet, Olivia Vénot, Pascal Tremblin, Nicolas Fray, Marie-Claire Gazeau, Martin Schwell, Antoine Jolly, et al.

► To cite this version:

Benjamin Fleury, Mathilde Poveda, Yves Benilan, Roméo Veillet, Olivia Vénot, et al.. High-temperature measurements of acetylene VUV absorption cross sections and application to warm exoplanet atmospheres. *Astronomy & Astrophysics - A&A*, 2025, 693, pp.A82. 10.1051/0004-6361/202451638 . hal-04863985

HAL Id: hal-04863985







<https://hal.science/hal-04863985v1>

Submitted on 4 Jan 2025

HAL is a multi-disciplinary open access archive for the deposit and dissemination of scientific research documents, whether they are published or not. The documents may come from teaching and research institutions in France or abroad, or from public or private research centers.

L'archive ouverte pluridisciplinaire **HAL**, est destinée au dépôt et à la diffusion de documents scientifiques de niveau recherche, publiés ou non, émanant des établissements d'enseignement et de recherche français ou étrangers, des laboratoires publics ou privés.

High-temperature measurements of acetylene VUV absorption cross sections and application to warm exoplanet atmospheres

Benjamin Fleury^{1,*}, Mathilde Poveda^{2,3}, Yves Benilan², Roméo Veillet¹, Olivia Venot¹,
Pascal Tremblin³, Nicolas Fray², Marie-Claire Gazeau², Martin Schwell², Antoine Jolly²,
Nelson de Oliveira⁴, and Et-touhami Es-sebbar⁵

¹ Université Paris Cité and Univ Paris Est Creteil, CNRS, LISA, 75013 Paris, France

² Univ Paris Est Creteil and Université Paris Cité, CNRS, LISA, 94010 Créteil, France

³ Université Paris-Saclay, UVSQ, CNRS, CEA, Maison de la Simulation, 91191 Gif-sur-Yvette, France

⁴ Synchrotron SOLEIL, L'Orme des Merisiers, 91192 Gif-sur-Yvette, France

⁵ Clean Energy Research Platform (CERP), Physical Sciences and Engineering Division, King Abdullah University of Science and Technology (KAUST), Thuwal 23955-6900, Saudi Arabia

Received 24 July 2024 / Accepted 21 November 2024

ABSTRACT

Context. Most observed exoplanets have high equilibrium temperatures ($T_{\text{eq}} > 500$ K). Understanding the chemistry of their atmospheres and interpreting their observations requires the use of chemical kinetic models including photochemistry. The thermal dependence of the vacuum ultraviolet (VUV) absorption cross sections of molecules used in these models is poorly known at high temperatures, leading to uncertainties in the resulting abundance profiles.

Aims. The aim of our work is to study experimentally the thermal dependence of VUV absorption cross sections of molecules of interest for exoplanet atmospheres and provide accurate data for use in atmospheric models. This study focuses on acetylene (C_2H_2).

Methods. We measured absorption cross sections of C_2H_2 at seven temperatures ranging from 296 to 773 K recorded in the 115–230 nm spectral domain using VUV spectroscopy and synchrotron radiation. These data were used in our 1D thermo-photochemical model, to assess their impact on the predicted composition of a generic hot Jupiter-like exoplanet atmosphere.

Results. The absolute absorption cross sections of C_2H_2 increase with temperature. This increase is relatively constant from 115 to 185 nm and rises sharply from 185 to 230 nm. The abundance profile of C_2H_2 calculated using the model shows a slight variation, with a maximum decrease of 40% near 5×10^{-5} bar, when using C_2H_2 absorption cross sections measured at 773 K compared to those at 296 K. This is explained by the absorption, higher in the atmosphere, of the actinic flux from 150 to 230 nm due to the increase in the C_2H_2 absorption in this spectral range. This change also impacts the abundance profiles of other by-products such as methane (CH_4) and ethylene (C_2H_4).

Conclusions. We present the first experimental measurements of the VUV absorption cross sections of C_2H_2 at high temperatures. Similar studies of other major species are needed to improve our understanding of exoplanet atmospheres.

Key words. astrochemistry – molecular data – methods: laboratory: molecular – techniques: spectroscopic – planets and satellites: atmospheres

1. Introduction

With current observational constraints, a large fraction of observed exoplanets whose atmospheres can be studied with spectroscopy orbits close by their host star, receiving a high stellar flux and exhibiting elevated equilibrium temperatures ($T_{\text{eq}} > 500$ K). In particular, the high flux received in the ultraviolet (UV) has important implications for the composition of the atmosphere of these planets. Indeed, vacuum ultraviolet (VUV) photons (i.e., photons with wavelengths shorter than 200 nm) modify the composition of planetary atmospheres by photodissociating atmospheric constituents, and thus initiating photochemical reactions (Moses 2014). While this process has been expected and predicted by photochemical models (Line et al. 2010, 2011; Moses et al. 2011; Venot et al. 2015, 2020; Baeyens et al. 2022), only recent observations of the warm gas giants WASP-39b and WASP-107b by JWST have provided the first direct evidence of the presence of photochemistry and its

impact on the composition of observed exoplanet atmospheres (Tsai et al. 2023; Dyrek et al. 2024). Indeed, spectral signatures assigned to sulfur dioxide (SO_2) (Alderson et al. 2023; Dyrek et al. 2024; Powell et al. 2024) have been observed for the first time in these atmospheres with JWST. The presence of this compound has been explained by 1D thermo-photochemical models, as a result of a consecutive series of chemical reactions initiated by photochemistry (Tsai et al. 2023; Dyrek et al. 2024). Therefore, it is now obvious that understanding exoplanet atmospheres and interpreting their observations requires the use of kinetic models that incorporate photochemistry.

To implement photochemistry, 1D thermo-photochemical models require the VUV absorption cross sections of molecules present in exoplanetary atmospheres as input parameters. These data are essential for calculating radiative transfer through the atmosphere and subsequently determining molecular photodissociation rates as a function of altitude. To obtain accurate results, these models need to use data suitable for the appropriate conditions (i.e., temperature, pressure, etc.) encountered in

* Corresponding author; benjamin.fleury@lisa.ipsl.fr

Table 1. VUV and UV absorption cross sections of C₂H₂ previously reported in the literature.

Temperature (K)	Spectral range (nm)	Resolution (nm)	References
85	110–155	0.02	Cheng et al. (2011)
150	120–215	0.007	Wu et al. (2001)
155	153–193	0.08	Wu et al. (1989)
	140–210	0.007	Chen et al. (1991)
173	185–235	0.02	Bénilan et al. (2000)
193	190–247	0.0001	Watson et al. (1982)
195	147–201	<0.0075	Smith et al. (1991)
	106–180	0.1	Nakayama & Watanabe (1964)
Ambient	165–195		Foo & Innes (1973)
	190–247	0.0001	Watson et al. (1982)
	105–155	0.04	Suto & Lee (1984)
	193–219	0.0001	Van Craen et al. (1985, 1986)
	153–193	0.08	Wu et al. (1989)
	137–201	<0.0075	Smith et al. (1991)
	200–400	0.5	Vattulainen et al. (1997)
	185–235	0.02	Bénilan et al. (2000)
	120–230	0.007	Wu et al. (2001)
	105–153	0.08	
	116.9–117.5	0.0012	Boyé et al. (2004)
	110–155	0.02	Cheng et al. (2011)
370	200–300	3.5	Zabeti et al. (2017)
	120–140	0.007	Wu et al. (2001)
873, 1073	200–400	0.5	Vattulainen et al. (1997)
565–1500	200–300	3.5	Zabeti et al. (2017)

these environments, which are often not comparable to the Solar System. Indeed, uncertainties in these data lead to uncertainties in the molecular abundances predicted by atmospheric models (Venot et al. 2013, 2018; Ranjan et al. 2020). In general, the thermal dependence of the VUV absorption cross sections of molecules is poorly known for the range of temperature observed in exoplanet atmospheres. Indeed, most of the corresponding studies are limited to the relatively low temperatures ($T < 400$ K) of the atmospheres of the Solar System but do not extend to the higher temperatures observed in extrasolar atmospheres (500 – 2000 K). These studies concern various molecules such as SO₂ (Wu et al. 2000; Rufus et al. 2009), methane (CH₄) and ethane (C₂H₆) (Chen & Wu 2004), ethylene (C₂H₄) (Wu et al. 2004), or ammonia (NH₃) (Cheng et al. 2006; Wu et al. 2007). In addition, studies have also been conducted to measure the absorption cross sections of some molecules such as acetylene (C₂H₂) (Vattulainen et al. 1997; Zabeti et al. 2017), ammonia (NH₃) (Weng et al. 2021), hydrogen sulfide (H₂S), carbon disulfide (CS₂), and carbonyl sulfide (OCS) (Grosch et al. 2015) at elevated temperatures up to 1500 K, but these measurements are limited to wavelengths longer than 200 nm. However, Venot et al. (2013, 2018) have measured the absorption cross section of carbon dioxide (CO₂) across a wider range of temperatures (150 to 800 K) and in a wavelength range critical for photochemistry (115–230 nm). Their studies show that its absorption cross section varies by several orders of magnitude with the temperature. Overall, this demonstrates the need to measure the absorption cross sections of molecules of interest for exoplanetary atmospheres at higher temperatures, as has been highlighted in collaborative white papers (Fortney et al. 2019; Chubb et al. 2024).

In this study, we investigate the thermal dependence of the VUV absorption cross section of acetylene. Although C₂H₂ detection has been claimed in only one observation of the

atmosphere of HD 209458b (Giacobbe et al. 2021), theoretical models predict that it is one of the major products of methane photochemistry in gas giant exoplanet atmospheres (Moses et al. 2013b; Venot et al. 2015; Kawashima & Masahiro 2018; Baeyens et al. 2022), making this molecule a possible indicator of disequilibrium chemistry. Moreover, the C₂H₂ mixing ratio could be used as an indicator of the atmospheric carbon-to-oxygen ratio (C/O), as the abundance of this molecule is expected to increase significantly in atmospheres with C/O > 1 (Moses et al. 2013a; Venot et al. 2015; Rocchetto et al. 2016; Drummond et al. 2019).

Numerous experimental measurements of the UV absorption cross section of C₂H₂ have been conducted, covering a wide range of wavelengths in the VUV (from 110 to 200 nm) as well as in the mid-UV and near-UV up to 400 nm (Nakayama & Watanabe 1964; Foo & Innes 1973; Watson et al. 1982; Suto & Lee 1984; Van Craen et al. 1985, 1986; Wu et al. 1989; Chen et al. 1991; Smith et al. 1991; Vattulainen et al. 1997; Bénilan et al. 2000; Wu et al. 2001; Boyé et al. 2004; Cheng et al. 2011; Zabeti et al. 2017). Table 1 provides a summary of the temperature, spectral range, and resolution used in some of these previous studies.

As is shown in Table 1, most of these measurements have been conducted at ambient temperature (~295 K) or at lower temperatures relevant to the atmospheres of other Solar System objects where C₂H₂ has been observed, such as the gas giants (Ridgway 1974; Moos & Clarke 1979; Orton et al. 1987; Herbert et al. 1987; Macy 1980), Titan (Hörst 2017; Nixon 2024) and Pluto (Stern et al. 2015). Only a few measurements have been conducted at higher temperatures. Wu et al. (2001) measured the absorption cross section of C₂H₂ from 120 to 140 nm at 370 K and observed an average increase of 20% in the absorption cross section compared to data at 295 K. Vattulainen et al. (1997) measured the absorption cross section of C₂H₂ between 200 and 400 nm at ambient temperature, 873 K, and 1073 K and

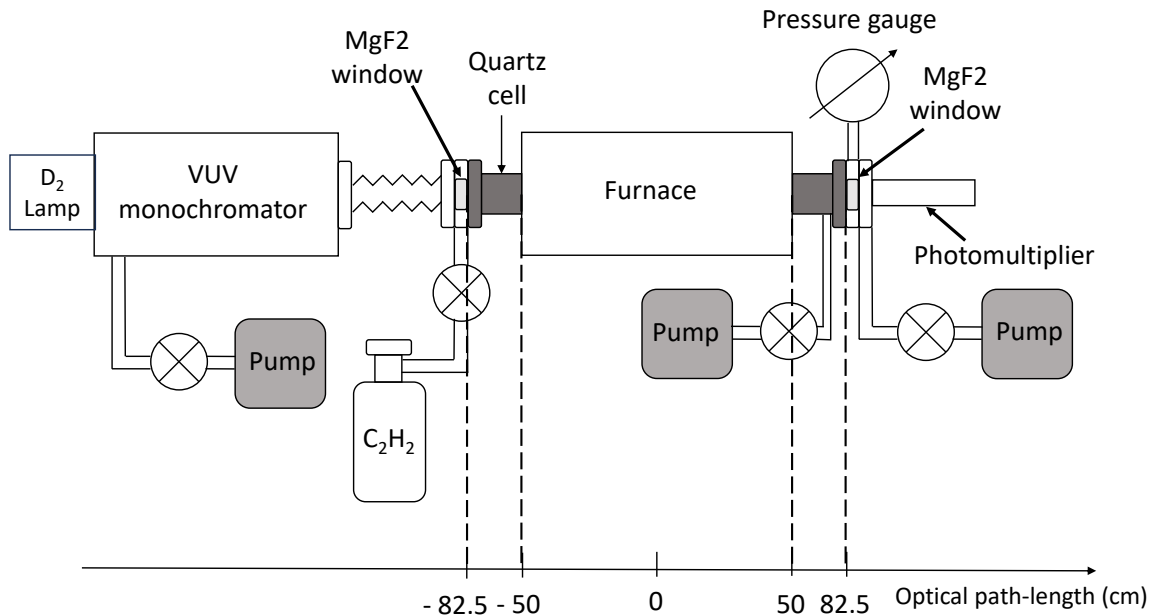


Fig. 1. Experimental setup used at LISA to measure the VUV spectra of acetylene.

showed an increase of up to a factor of ten in the cross section with temperature. Finally, Zabeti et al. (2017) have measured the absorption cross section from 200 to 300 nm, of shocked heated C_2H_2 in the 565–1500 K temperature range. The authors also observed an increase in the absorption cross section with temperature as well as a shift of the maximum of the absorption toward longer wavelengths. There is, therefore, no existing data on the absorption cross section of C_2H_2 for both the range of temperatures and the whole VUV spectral domain that would be relevant for modeling the photochemistry in exoplanet atmospheres.

In this paper, we present a study of the thermal dependence of the VUV absorption cross section of C_2H_2 from 296 to 793 K and for a large spectral domain ranging from 115 to 230 nm. Thus, our study encompasses most of the spectral domain of C_2H_2 photodissociation, which extends from the photodissociation threshold at 5.71 eV (217 nm) to the photoionization threshold at 11.27 eV (110 nm) (Heays et al. 2017). In Sect. 2, we describe the new UV spectroscopy platform used to determine the absorption cross section of C_2H_2 . Our measurements, their analyses, and the atmospheric simulations to quantify the impact of these new data on the abundances predicted by thermo-photochemical models are presented in Sect. 3. Finally, the conclusions of this study are summarized in Sect. 4. The C_2H_2 absorption cross section data measured in this study can be downloaded from the ExoMol database (Tennyson et al. 2024)¹ and the ANR EXACT project website².

2. Experimental methods and protocols

2.1. Measurements of acetylene UV absorption spectra

The absorption spectra of gaseous acetylene were measured at high temperatures using a new custom-made VUV spectroscopy platform developed at the Laboratoire Interuniversitaire des Systèmes Atmosphériques (LISA, France). A scheme of the experimental setup is presented in Fig. 1.

¹ <https://www.exomol.com>

² <https://www.anr-exact.cnrs.fr/fr/absorption-cross-sections>

The setup consists of a high-temperature absorption cell composed of a quartz tube sealed at each extremity with magnesium fluoride (MgF_2) windows (16 mm in diameter) mounted on stainless-steel flanges. The optical pathlength of the cell was 165 cm. The cell was installed in a furnace that can warm up to 1373 K. The temperature of the cell was continuously measured with three type-K thermocouples equally spaced along its length. Before each measurement at a given temperature, the cell was pumped using a turbomolecular pump and heated up to the studied temperature for 24 hours to desorb and evacuate gases. At ambient temperature, the background pressure was 10^{-7} mbar. For this study, spectra were measured at ambient temperature (i.e., 296 K) as well as at 373, 473, 573, 673, and 773 K. We limited our measurements to a maximum temperature of 773 K due to rapid thermal decomposition of C_2H_2 observed at elevated temperatures, probably enhanced by catalytic processes onto the surface of the cell (see discussion in Sect. 3.2).

The VUV spectra of C_2H_2 were measured from 115 to 230 nm using a McPherson 225 ultrahigh vacuum (UHV) monochromator (1 m focal length) pumped down to 8×10^{-8} mbar using an ionic pump to prevent absorption by atmospheric molecules (nitrogen, N_2 , oxygen, O_2 , etc.). The limits of the wavelength range are due, respectively, to the MgF_2 windows cut-on and the first order diffraction grating's limit. At the entrance of the monochromator, a 30 W deuterium (D_2) lamp produces a polychromatic VUV-UV beam directed toward the diffraction grating (1200 slits/mm, blazed at 140 nm), which reflects and disperses the light to obtain a quasi-monochromatic beam at the exit slit. Then, the beam passes through the cell and the photons are detected by a Hamamatsu R6836 photomultiplier tube producing a current proportional to the photon flux. Finally, the current is measured and digitalized using a Keithley 6485 pico-amperemeter. The entrance and exit of the monochromator are equipped with slits and occulters. The height of occulters can be adjusted from 2 to 20 mm and the width of slits from 0.005 to 2 mm. For this study, entry and exit occulter heights were set respectively to 6 and 4 mm, while both the entry and exit slits' widths were set to 40 μm . With these slits' width, the spectral resolution of the monochromator, which corresponds to the full

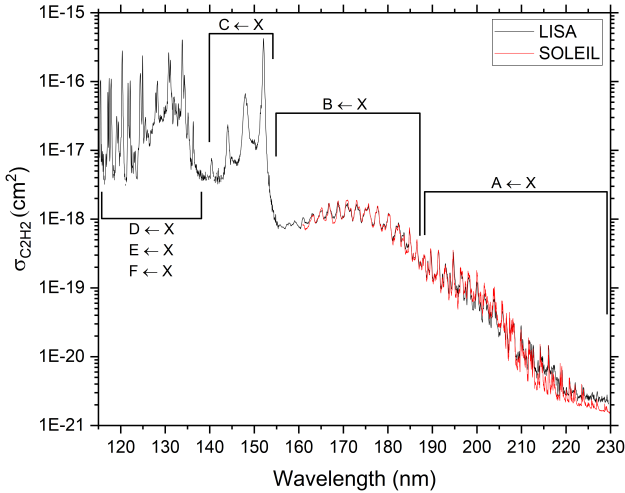


Fig. 2. Absorption cross section of C_2H_2 determined from 115 to 230 nm at LISA (black) and from 160.8 to 230 nm at SOLEIL with a resolution of 0.1 nm (red). Electronic transitions associated with observed absorption bands are indicated.

width at half maximum of a spectral band, is 0.034 nm. However, this spectral resolution was further limited to ~ 0.1 nm by the chosen sampling interval (one point every 0.03 nm). In the case of measurements using the LISA setup, a background spectrum with an empty cell was recorded at the beginning of each measurement, followed by the acquisition of various absorption spectra for C_2H_2 . The background spectrum was obtained after allowing the D_2 lamp to warm up for at least one hour. We noted that during the first hour after being turned on, the emission intensity of the D_2 lamp could fluctuate by a few percent. After this initial warm-up period, the emission intensity stabilizes sufficiently, contributing only slightly to the uncertainty, which is accounted for in the measured spectra.

As the acetylene cross section spans a variation of five orders of magnitude in the studied spectral domain (see Fig. 2), it was necessary to employ a wide range of pressures to accurately record the smallest absorptions and prevent any saturation of the strongest absorption bands. To facilitate our measurements, we divided the full wavelength range into ten overlapping segments of a few nanometers each. For each measurement, gaseous acetylene (Air Liquide, purity $>99.5\%$) was introduced into the cell at the desired pressure (ranging from 10^{-3} to 80 mbar) and all the considered segments were measured at least three times at different pressures. In total, fifty spectra were measured at each temperature. The absolute pressure of C_2H_2 in the cell was measured with two capacitance gauges ranging from 10^{-4} to 1 mbar and from 0.1 to 1000 mbar, respectively. As was discussed in Bénilan et al. (1995), the presence of acetone traces inside the gas cylinder (used as a stabilizer) can affect the spectra of C_2H_2 recorded in certain part of the VUV domain (~ 185 – 196 nm) where acetone cross sections (Nobre et al. 2008) are large compared to acetylene ones. To prevent this issue when measuring the corresponding spectral domain, acetone present in the injected gas was removed by circulating the gas before injection into a cold trap made of a stainless-steel coil immersed in a slush of liquid nitrogen and acetone at ~ 183 K.

Additional spectra of C_2H_2 were measured at 296, 573, and 773 K at synchrotron SOLEIL (proposal 20150691, PI: Venot) on the DESIRS (Dichroïsme Et Spectroscopie par Interaction avec le Rayonnement Synchrotron) VUV beamline, whose wavelength range extends from 30 to 250 nm (Nahon et al. 2012).

Although mostly similar, the method employed at SOLEIL presented a few differences. Firstly, measurements were made using a metallic cell made of Kanthal material (instead of quartz) with a shorter optical pathlength of 146 cm. This cell was used previously to measure CO_2 spectra (Venot et al. 2013, 2018). Second, DESIRS beamline is equipped with a Fourier Transform Spectrometer (FTS) that allows to record spectra at higher resolution (resolving power up to $\sim 10^6$) and with a high absolute wavelength accuracy of 1×10^{-7} (de Oliveira et al. 2011). At 296 K, spectra were measured from 160.82 to 196.08 nm with a resolution of 0.0134 nm and from 196.08 to 235.43 nm with a resolution of 0.0034 nm. At 573 and 773 K, spectra were measured from 154.37 to 169.49 nm with a resolution of 0.0537 nm and from 169.49 to 203.75 nm with a resolution of 0.0134 nm.

2.2. Data processing

2.2.1. Calculation of the absorption cross section

The absolute absorption cross section of C_2H_2 was calculated from the measured spectra using the Beer-Lambert law:

$$\sigma(\lambda, T) = \frac{1}{nL} \times \ln\left(\frac{I}{I_0}\right), \quad (1)$$

where $\sigma(\lambda, T)$ is the absorption cross section (cm^2) at a given wavelength, λ , and temperature, T , L is the optical pathlength (cm), n the volume density of the gas in the cell (cm^{-3}), I_0 the intensity of the light transmitted through an empty cell, and I the intensity of the light transmitted through the cell containing a density n of gas. Considering the gas as a perfect gas, the density of the gas in the cell can be calculated using the equation $n = P/k_B T$, where P is the pressure of C_2H_2 inside the cell (Pa), T the temperature (K), and k_B the Boltzmann constant.

Prior calculating the absorption cross section, it is necessary to eliminate data points from each measured spectrum that are too noisy (for low pressure) or saturated (for high pressure) by applying two filters. The first filter eliminates noisy points with a transmission higher than a fixed value (typically 80%). The second filter removes saturated points whose optical depth does not increase linearly with the gas pressure. Then, for the ten segments and each pressure, the absorption cross section was calculated using Eq. (1) and a mean value was determined. Finally, the ten spectra obtained were concatenated to reconstruct the full spectrum ranging from 115 to 230 nm.

2.2.2. Temperature and wavelength calibrations

The temperature gradient along the entire absorption cell was quantified in our previous studies by Venot et al. (2013, 2018), which examined the effect of high temperature on the VUV cross sections of CO_2 molecules. The temperature reaches its peak at the cell center, equal to the set oven temperature, and then symmetrically decreases toward near-ambient at the cell edges. Near the center, the temperature remains maximal over a length of about 35 cm. The transition section, where the temperature drops from maximum to ambient, spans approximately 25 cm in length, while the zones near ambient temperature are roughly 22.5 cm. As the absorption is dominated by the gas at high temperature, to calculate the gas density and then the absorption cross section, we decided to follow the same assumption as in Venot et al. (2018) and to consider that the temperature of the gas is equal to the maximum temperature (T_{max}) all along the optical pathlength. The measurement uncertainties in the absorption

cross sections of C_2H_2 were determined using a root-sum-of-squares analysis, as was described by [Meyn \(2000\)](#); [Es-sebbar & Farooq \(2014\)](#). According to Eq. (1), the uncertainty contributions considered from different sources, include concentration (i.e., impurities) $\Delta n/n$, optical path length $\Delta l/l$, temperature $\Delta T/T$, pressure $\Delta P/P$, and measured absorbance $\Delta A/A$. The concentration uncertainty was estimated to be under 0.5%, primarily due to a maximum of 0.5% impurities, possibly acetone, present in the acetylene gas cylinder ([Bénilan et al. 1995](#)). The uncertainty in the optical path length was calculated to be less than 1%. This was determined by comparing absorption data measured at room temperature in two absorption cells with optical path lengths of 165 cm and 146 cm at LISA and SOLEIL, respectively. The pressure measurement, considering both the manufacturing accuracy of the Baratron capacitance manometers and minor pressure variations during recording, particularly at high resolution, has an estimated relative uncertainty of 0.5%. The error in the absorbance ranged from 1 to 2%, which also accounts for the slight variations in the background intensity of the D_2 lamp. At ambient temperature, the temperature uncertainty in the cell yields a relative uncertainty of $\Delta T/T \sim 0.5\%$. Overall, uncertainty in the measured cross sections at ambient temperature is estimated to be below 6%, accounting for all sources of error. However, at high temperatures, temperature gradients become a significant source of uncertainty among all contributing factors, as the temperature is not uniform along the absorption cell. This temperature variation induces changes in gas density along the cell while pressure remains constant. Subsequently, the uncertainty in the absorption measured at a given maximum temperature, T_{\max} , largely depends on the variation in the absorption cross section of C_2H_2 between the cooler and warmer regions of the cell. More recently, [Poveda \(2023\)](#) investigated the effect of temperature gradients on the measured absorption cross sections of CO. This study demonstrated that most of the absorption from the hot bands occurs within a ± 40 cm region at the center of the cell, where the temperature is highest, promoting the formation of hot bands. Consequently, the temperature gradient introduces only a minor additional uncertainty to the measured cross section for these hot bands. However, the results of our study provide limited information on the cold bands. Assuming equal lengths for the cold and warm sections of the cell, the column density would vary as $1/T$. With a gas temperature roughly twice as high at the center compared to the extremities of the cell, the column density would be approximately twice as high in the colder section. This could lead to an underestimation of the absorption cross section at high temperature by several tens of percent. Further work is needed to more precisely evaluate the uncertainty introduced by the temperature gradient.

The wavelength calibration of the spectra measured at LISA was carried out on the basis of the spectra measured at SOLEIL because of the high absolute wavelength accuracy of the spectra measured with the FTS of the DESIRS beamline ([de Oliveira et al. 2011](#)). For the comparison and calibration purpose of the spectra, it was necessary to first degrade the SOLEIL spectra to the lower resolution used at LISA (0.1 nm).

3. Results and discussions

3.1. Absorption cross sections of C_2H_2 at 296 K

3.1.1. New data obtained at LISA and SOLEIL facilities

We started our study by measuring the absorption cross section of C_2H_2 at 296 K. Data obtained at LISA from 115 to 230 nm

as well as the ones obtained at SOLEIL (after degrading the resolution of the spectrum to 0.1 nm) from 160.82 to 230 nm are presented in Fig. 2. The spectra present two components: a continuum and different band systems superimposed on it. Band's features observed from 185 to 230 nm and from 153 to 185 nm are attributed, respectively, to the $A^1A_u \leftarrow X^1\Sigma_g^+$ and $B^1B_u \leftarrow X^1\Sigma_g^+$ electronic transitions from the ground state X to the two first excited states A and B ([Foo & Innes 1973](#); [Watson et al. 1982](#); [Van Craen et al. 1985, 1986](#); [Wu et al. 1989](#); [Chen et al. 1991](#); [Smith et al. 1991](#)). Sharp and intense absorption bands from 140 to 155 nm are attributed to the $C^1\Pi_u \leftarrow X^1\Sigma_g^+$ electronic transition to the C Rydberg state ([Herzberg 1966](#); [Gedanken & Schnepf 1976](#)). Finally, absorption bands observed at wavelengths shorter than 140 nm are attributed to the $D^1\Sigma_u^+ \leftarrow X^1\Sigma_g^+$, $E^1\Pi_u \leftarrow X^1\Sigma_g^+$, and $F^1\Pi_u \leftarrow X^1\Sigma_g^+$ electronic transitions involving the D and F Rydberg states as well as the E valence state ([Wu et al. 2001](#); [Boyé et al. 2004](#); [Cheng et al. 2011](#)). In general, the two sets of data agree in terms of absolute values of the intensity, but we observed some differences in the continuum level of the $A \leftarrow X$ system. From 195 to 205 nm, the SOLEIL values are higher than LISA ones, while from 210 to 230 nm, the continuum level is lower in the SOLEIL spectrum than in the LISA one. Nevertheless, in both cases, there is $\sim 25\%$ of differences between the continuum values. In addition, we also observed in this 195–205 nm region that the absorption bands in the LISA spectrum are less intense than those in the SOLEIL spectrum. The origin of these differences is difficult to establish, but we can formulate some hypothesis. Firstly, we observe that the region where the intensity of the SOLEIL spectrum is more intense than the LISA one (195 to 205 nm) corresponds to the region for which the acetone traces present inside the gas cylinder absorbs and, thus may affects the calculation of the absorption cross section of C_2H_2 ([Bénilan et al. 1995](#)). Therefore, our result may suggest that the acetone have not been totally trapped in one of the experiments, resulting in an additional absorption in this spectral region. For the 210–230 nm region, we note that the pressures used at SOLEIL and LISA are not identical. Higher pressures were used for some of the SOLEIL spectra compared to those of LISA. If the pressures used at LISA were too low, it may lead to a higher noise level on the continuum, resulting in a higher uncertainty on the intensity of the continuum in this region. The high-resolution spectrum obtained at SOLEIL, presented in Fig. 3, reveals that at longer wavelengths (i.e., $\lambda > 185$ nm), corresponding to the C_2H_2 ($A \leftarrow X$) band system, rotational structures are well resolved. However, at shorter wavelengths below 185 nm, predissociation causes a broadening and a decrease in absorption intensity, resulting in bands without visible rotational features. In the lower-resolution LISA spectrum, only the predissociation-broadened bands are resolved and distinguishable, while the rotational structures at longer wavelengths are no longer resolved.

3.1.2. Comparison with data available in the literature

We compare in Fig. 4 the absorption cross section measured at ambient temperature with data available in the literature ([Smith et al. 1991](#); [Bénilan et al. 2000](#); [Cheng et al. 2011](#)) and which cover the whole wavelength range of our study (i.e., 115–230 nm). For $115 < \lambda < 185$ nm, our data generally agree with the ones measured by [Smith et al. \(1991\)](#); [Cheng et al. \(2011\)](#) despite observing some differences in the intensity of the baseline, especially for $\lambda < 140$ nm as well as around, 145, and 155 nm. We note that ~ 155 nm, the continuum in LISA spectrum does not decrease as much as in [Smith et al. \(1991\)](#); [Cheng et al. \(2011\)](#)

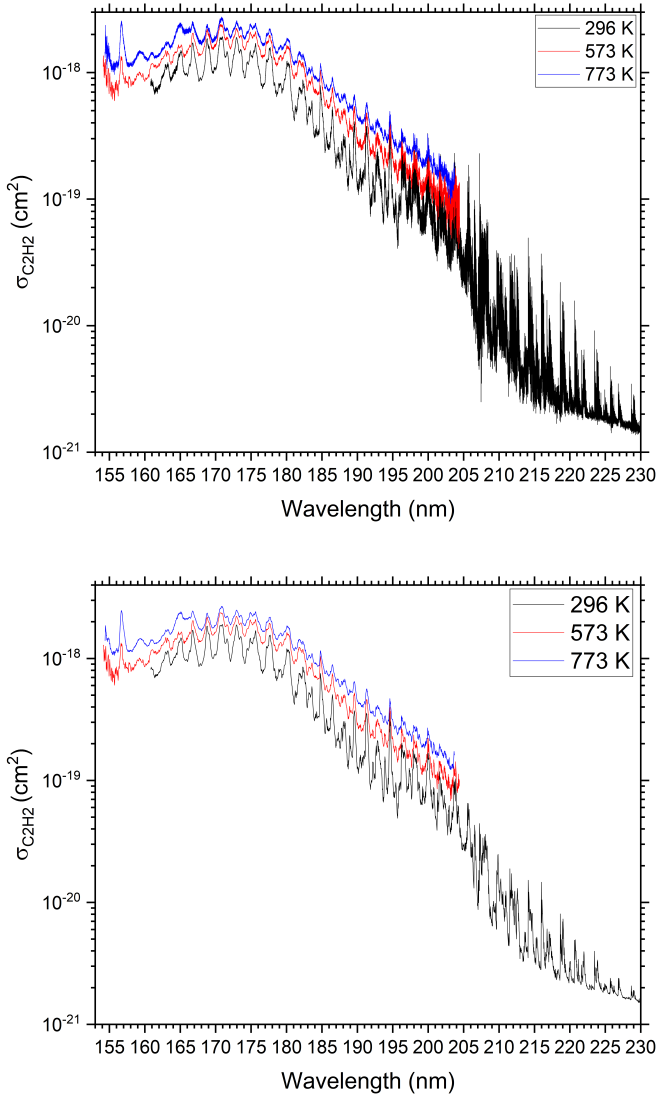


Fig. 3. Absorption cross section of C_2H_2 measured at synchrotron SOLEIL from ~ 154 to 230 nm at 296 K (black), 573 K (red), and 773 K (blue). Top: spectra measured at SOLEIL with resolutions ranging from 0.0134 to 0.0034 nm. Bottom: same spectra after a degradation of their resolution to 0.1 nm (the one used at LISA).

toward longer wavelengths. As was mentioned previously, these differences could be explained by using lower pressures in this spectral range, impacting the accurate determination of the continuum intensity. Additionally, the LISA spectra exhibit a slight noise around 155 nm due to numerous emission bands from the D_2 lamp (used as light source), particularly the large emission from 155 to 165 nm features of molecular D_2 ($B^1\Sigma_u \leftarrow X^1\Sigma_g$). Yet, these bands are not resolved with the settings used for our measurements. In addition, the intensity of those bands may vary of a few percent over time due to variations in the lamp's temperature. Subsequently, this contributes to a slight increase in the noise level and uncertainty of the intensity of the continuum in this region.

From 185 to 195 nm, our data agree with [Bénilan et al. \(2000\)](#) but we observe important differences compared to the data from [Smith et al. \(1991\)](#), which exhibit two large absorption bands that are absent from the other spectra. As was described in Sect. 2.1, we suppose that these bands are due to the contamination of C_2H_2 by acetone ([Bénilan et al. 1995](#)), which was not

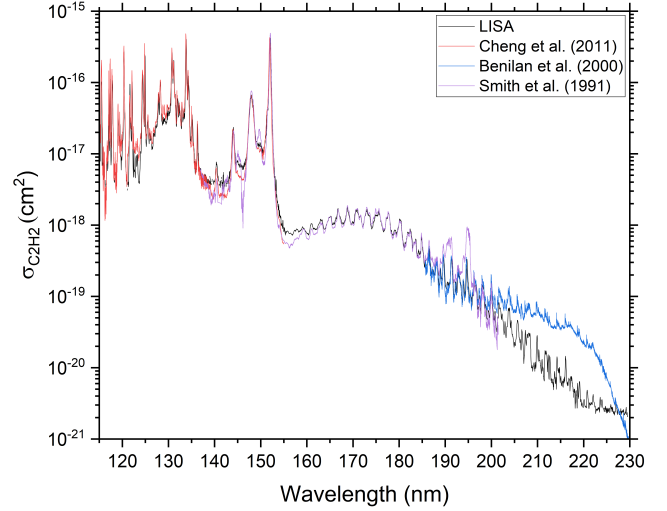


Fig. 4. Comparison of absorption cross of C_2H_2 section measured at ambient temperature from 115 to 230 nm at LISA (black) with the ones measured by [Cheng et al. \(2011\)](#) (red), [Smith et al. \(1991\)](#) (purple), and [Bénilan et al. \(2000\)](#) (blue).

trapped in the study by [Smith et al. \(1991\)](#) contrary to our measurements and those of [Bénilan et al. \(2000\)](#). Beyond 195 nm, we observed a good agreement between our data and those of [Smith et al. \(1991\)](#), which extends up to 200 nm. However, we observed important differences (up to one order of magnitude) with the data measured by [Bénilan et al. \(2000\)](#) from 195 to 230 nm. Indeed, while in our spectrum the intensity of the baseline continues to decrease exponentially from 195 to 230 nm, the intensity of the spectrum measured by these authors decreases much slowly up to 220 nm before decreasing drastically up to 230 nm. Although it is not possible to identify with certainty the origin of these differences, the higher absorption cross section determined by [Bénilan et al. \(2000\)](#) would suggest that the gas used by these authors could have been contaminated with another species that absorb at these wavelengths, leading to a bias in the determination of the absorption cross section of C_2H_2 in this spectral region.

3.2. Evolution of C_2H_2 absorption cross section with the temperature

Following the measurements at 296 K, we determined the absorption cross section of C_2H_2 at 373, 473, 573, 673, and 773 K. Figure 5 presents the evolution of the absolute absorption cross section of C_2H_2 measured from 115 to 230 nm at LISA as a function of temperature. In general, we observe an increase in the intensity of the continuum and a decrease in the intensity of the absorption bands as the gas temperature increase. This results in a net increase in the absolute absorption cross section of C_2H_2 with temperature. In the 160 to 230 nm range, the absorption cross section increases linearly with the temperature. However, we observe at 773 K a more important increase in the absorption cross section for wavelengths above 210 nm compared to the other temperatures, with the appearance of a bump centered at 222.5 nm. We were not able to determine the absorption cross section of C_2H_2 at higher temperature because we observed a fast thermal degradation at 873 K. As a result, the gas density inside the cell was not constant over time and could not be determined based on the measured gas pressure. Therefore, we could not calculate the absorption cross section of C_2H_2 at 873 K based on the

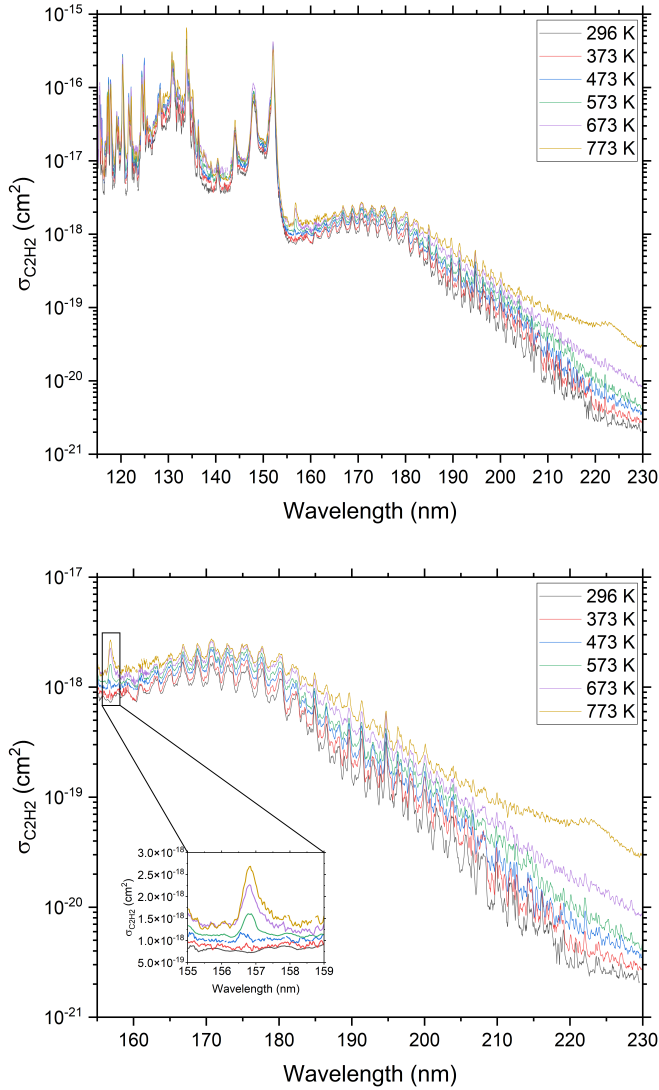


Fig. 5. Absorption cross section of C_2H_2 determined at LISA at 296 K (black), 373 K (red), 473 K (blue), 573 K (green), 673 K (violet), and 773 K (yellow). Top: spectra covering the whole studied spectral range from 115 to 230 nm. Bottom: same spectra with a focus on the 155–230 nm range and on the 155–159 nm range, as is shown in the inset.

spectra measured experimentally, and thus did not attempt to go to even higher temperatures. Due to the role of C_2H_2 in the formation of other hydrocarbons and soot in combustion systems, the thermal decomposition of C_2H_2 has been extensively studied. It has been observed that in static conditions (like the ones used in our experiments), acetylene pyrolysis can occur at temperatures lower than 1000 K (Duran et al. 1988; Colket et al. 1989; Kern et al. 1991; Benson 1992; Zádor et al. 2017; Liu et al. 2021). This agrees with our observations, where C_2H_2 thermal degradation may be further enhanced by the walls of the absorption cell. For temperatures lower than 1500 K, the mechanism responsible for the pyrolysis of acetylene has not been firmly established and different initiation reactions have been proposed, such as acetylene dimerization or self-reaction (Benson 1992; Zádor et al. 2017). Nevertheless, the thermal degradation of C_2H_2 can lead to the formation of new molecules such as polyacetylenes (Aghsaee et al. 2014), which may affect the absorbance measured experimentally resulting in an overestimation of the absorption cross section. This has been shown by Zabeti et al. (2017) who

determined experimentally the absorption cross section of C_2H_2 from 200 to 400 nm for temperatures up to 1500 K using a large shock tube facility. They reported values five times lower than those previously determined by Vattulainen et al. (1997). They concluded that the measurements of Vattulainen et al. (1997), conducted in static systems with longer residence times (a few minutes), were affected by the pyrolysis of C_2H_2 . In contrast, in the study reported by Zabeti et al. (2017), the effect of the thermal degradation of C_2H_2 was negligible, due to the much shorter residence time (a few μs). These two observations suggest that in the LISA experiments, the significant increase in the absorption cross section observed at 773 K above 210 nm could be attributed to the thermal degradation of C_2H_2 at this temperature and the formation of new absorbing species. Additional work will be needed to confirm this hypothesis by measuring the evolution of the gas composition inside the cell as a function of time at 773 K.

In addition to these general variations, we observe at 473 K and beyond that a new absorption band appears at ~ 156.7 nm (see inset in Fig. 5-bottom), with an intensity that increases with the temperature. We identify this band as a hot band apparently originating from the ν_2 vibrational mode ($\nu_2 = 1973.8$ cm^{-1}). Indeed, the origin of this transition is at $65\,860$ cm^{-1} (Gedanken & Schnepf 1976) while the hot band is at $63\,816$ cm^{-1} . Therefore, the two vibrational levels are separated by 1973 cm^{-1} , which corresponds to the vibrational mode ν_2 .

Figure 3 presents the absorption cross sections of C_2H_2 obtained at SOLEIL at 296, 573, and 773 K at high resolution (top) and after degrading the spectral resolution alike that of LISA spectra. Similar to LISA data, we observe an increase in the continuum intensity and a decrease in the intensity of the absorption bands when the temperature increases. Moreover, we observed the apparition of the same “hot band” at ~ 156.7 nm in the spectra recorded at 573 and 773 K. However, the spectra recorded at high temperatures at SOLEIL do not extend beyond 205 nm, which prevents the study of a large part of the $A \leftarrow X$ band system where we observed the most significant variation in the absorption cross section with temperature at LISA (see Fig. 5).

To go further in the quantification of the change in the absorption cross section with the temperature, we calculated the factor of changes of the cross section, defined by Wu et al. (2001).

$$F_T = \frac{\sigma_T - \sigma_{296K}}{\sigma_{296K}}, \quad (2)$$

where F_T is the factor of changes of cross section between the temperature, T , and our reference at 296 K, σ_T is the absorption cross section at T , and σ_{296K} is the absorption cross section at 296 K. A positive value corresponds to an increase in the cross section at T comparatively to 296 K, while a negative value corresponds to a decrease. The calculation of F_T for the absorption cross section obtained at LISA (116 to 229 nm) at the different temperatures is presented in Fig. 6. From 116 to 185 nm, which corresponds to the $B \leftarrow X$ transition at 185 nm, the continuum increase is relatively constant on the whole wavelengths range at a given temperature, while the intensity of the absorption bands decreases. At 373 K, the cross section of C_2H_2 increases with an average F_T of 0.2, similarly to the value found by Wu et al. (2001) from 120 to 140 nm at 370 K. For the continuum, this factor increases with temperature up to an average of 0.5 at 773 K, while variations in certain bands can be more significant, up to a factor of 3.5. Beyond 185 nm (see Fig. 6 top), F_T increases

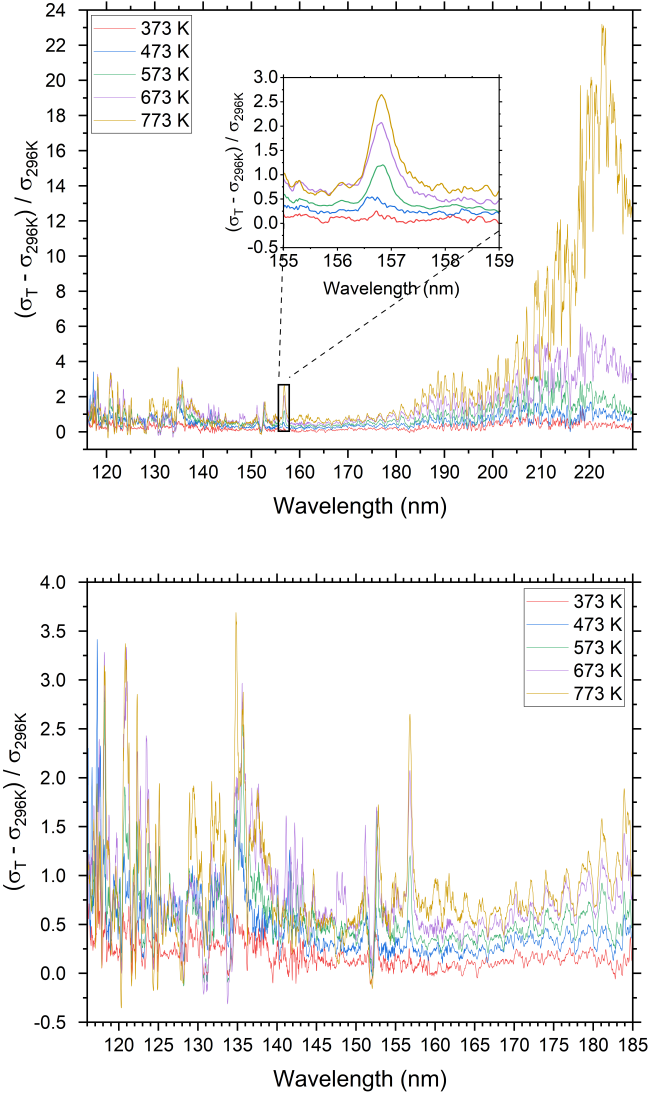


Fig. 6. Factor of changes, F_T , in the absorption cross section of C_2H_2 between high temperatures, T (K), and the ambient temperature (296 K) for LISA measurements. Top: F_T calculated for the whole studied spectral range (116 to 229 nm) along with an inset of 155–159 nm region where a hot band is visible. Bottom: same spectra showing only the 116 to 185 nm region.

sharply toward longer wavelengths until it reaches 195 nm, where it then decreases. Then, F_T rises sharply again along the C_2H_2 (A \leftarrow X) bands system until 215 nm, where another decrease is observed. Finally, F_T increases up to 220 nm before decreasing again until 230 nm.

This more important increase in the absorption cross section beyond 195 nm agrees with the presence of numerous hot bands identified in the A \leftarrow X bands system by [Watson et al. \(1982\)](#); [Van Craen et al. \(1985\)](#) and that we also observed in our spectra. Figure 7 presents the identification of numerous absorption bands of the A-X band system between 215 and 230 nm in our spectra measured at LISA and SOLEIL at ambient temperature. These bands involved the ν_4 vibrational mode in the $X^1\Sigma_g^+$ ground state and the ν_3 and $\nu_2 + \nu_3$ vibrational modes in the A^1A_u first excited state. We observed the presence of hot bands originating from the vibrational levels one and two of the ν_4 vibrational mode in the ground state. Additional hot bands were

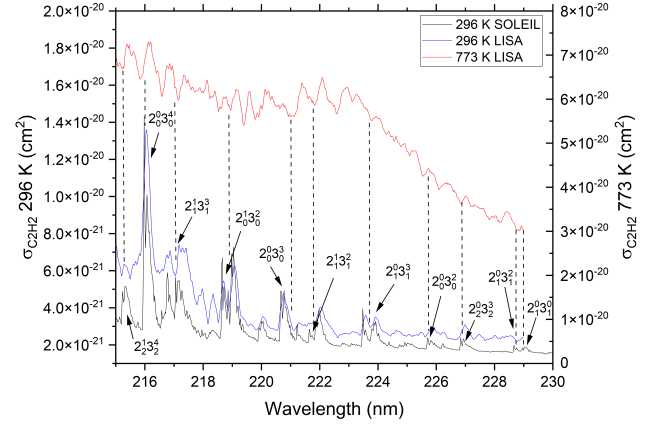


Fig. 7. Long wavelength region ($\lambda > 215$ nm) of the A-X band system of C_2H_2 measured at ambient temperature at SOLEIL (black) and LISA (blue) as well as measured at 773 K at LISA (red). Absorption bands in the ν_3 and $\nu_2 + \nu_3$ vibrational modes are identified based on the studies of [Watson et al. \(1982\)](#); [Van Craen et al. \(1985\)](#).

identified in the studies of [Watson et al. \(1982\)](#); [Van Craen et al. \(1985\)](#) but their intensities are very weak and cannot be observed in our spectra. As is shown in Fig. 7, at 773 K, we observed an increase in the continuum intensity compared to ambient temperature and a change in the contrast between cold and hot bands. Indeed, we observe an increase in the intensity of the hot bands regardless of the cold bands. Unfortunately, as the spectra measured by [Zabeti et al. \(2017\)](#) are not available, a full and detailed comparison with these data at high temperature is not possible. Nevertheless, we can observe that the cross section at 200 nm measured by these authors at 296 K ($\sim 3 \times 10^{-20}$ cm²) and 565 K ($\sim 4.5 \times 10^{-20}$ cm²) are lower by a factor of three compared to those measured at LISA (i.e., at 296 K, $\sim 7.5 \times 10^{-20}$ cm² and at 573 K $\sim 1.5 \times 10^{-19}$ cm²). Finally, we observe that at 773 K, from 215 to 220 nm, the F_T increases much faster than at lower temperatures, but as was discussed earlier, the thermal decomposition of C_2H_2 could bias the results at this higher temperature.

Figure 8 presents a comparison of F_T values calculated at 573 and 773 K from 160 to 204 nm using LISA and SOLEIL data. At 573 K, F_T values from LISA data agree well with those from SOLEIL data. At 773 K, the F_T values calculated from the two datasets agree up to 195 nm. However, for longer wavelengths, we observe some discrepancies, where F_T being more significant in LISA data than in SOLEIL ones. These discrepancies can be explained by the variation in the absorption cross section measured at ambient temperature (see Sect. 3.1.1), which is inferred in the calculation of F_T .

3.3. Application to exoplanet atmospheres

3.3.1. 1D thermo-photochemical model

We used the 1D thermo-photochemical model FRECKLL ([Al-Refaie et al. 2024](#); [Veillet et al. 2024](#)) to study and quantify the impact of the new C_2H_2 absorption cross sections data on the predicted atmospheric composition of exoplanets. We chose to model a hypothetical hot-Jupiter with a solar metallicity ([Lodders 2010](#)) and a C/O ratio twice the solar one. From a pure modeling point of view, such an assumption allows us to obtain a high amount of acetylene in the atmosphere of the planet, which is essential to evaluate the effect of our new data. Indeed, several studies have shown that the C_2H_2 abundance is enhanced in warm exoplanet atmospheres for a C/O ratio greater than

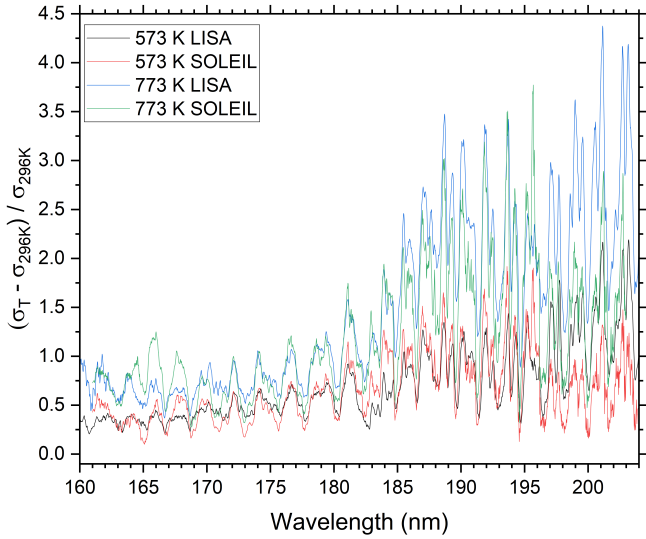


Fig. 8. Comparison of the factor of changes of the absorption cross section of C_2H_2 for the measurements made at 573 and 773 K at LISA and at SOLEIL from 160 to 204 nm.

one (Madhusudhan 2012; Moses et al. 2013b; Venot et al. 2015; Rocchetto et al. 2016). Such an assumption is also relevant given the large variety of elemental chemical abundances possible for exoplanet atmospheres (Madhusudhan et al. 2011; Moses et al. 2013a; Hu et al. 2015; Cridland et al. 2019; Tsai et al. 2021; Guzmán-Mesa et al. 2022).

We used the thermal profile published by Venot et al. (2015) and calculated with the analytical model of Parmentier & Guillot (2014), with an irradiation temperature (as defined by these authors) of 2303 K, leading to a high-altitude atmospheric temperature of 1500 K (Fig. 2 of Venot et al. 2015). While this temperature is higher than the one at which the cross section of C_2H_2 was measured, we made this choice to ensure an important amount of C_2H_2 in the upper atmosphere and thus optimize our analysis. To this end, we also tried to maximize the photolysis process and considered that our planet was orbiting a F-type star (Sect. 3.3.3). Our case-study planet has a radius $R = 1.25 R_{Jup}$, a mass $m = 1.5 M_{Jup}$, and a gravity $g = 25 \text{ m s}^{-2}$. Given the stellar irradiation, the semi-major axis has been fixed to $a = 0.05735 \text{ AU}$ to obtain an irradiation temperature of 2303 K. We assumed an Eddy diffusion coefficient constant with altitude $K_{zz} = 10^8 \text{ cm}^2 \text{ s}^{-1}$. We detailed hereafter the chemical scheme, and the irradiation spectra used in our model.

3.3.2. Chemical scheme

The model implements the chemical scheme from Veillet et al. (2024), which includes 175 species composed of C, N, H, and O elements and involved in 2550 reactions (1237 reversible and 76 irreversible). The scheme also includes 65 reactions of photodissociation. This scheme has been validated for a large range of pressures and temperatures through an extensive comparison with experimental combustion data (Veillet et al. 2024). It is therefore very robust and well suited to model warm atmospheres.

3.3.3. Stellar irradiation

The stellar spectrum of the exoplanet host star is an important input that allows one to model photolysis process, and thus

calculate the photodissociation rates of atmospheric molecules. As in Venot et al. (2018), we used a stellar spectrum of HD 128167 (F2V), which was constructed thanks to observational data of this star from 115 to 900 nm (Segura et al. 2003). For the shorter wavelengths (1–114 nm), we used data from the Sun (Thuillier et al. 2004), scaled to the effective temperature and radius of HD 128167 ($T = 6723 \text{ K}$ and $R = 1.434 R_{Sun}$).

3.3.4. C_2H_2 absorption cross section

We modeled the chemical composition of the atmosphere of our hypothetical planet using the absorption cross section of C_2H_2 measured in this study (see Sect. 3.2). To evaluate the effect of the thermal dependence of absorption cross sections, we ran two sets of simulations. From 7 to 115 nm, we used in both cases the absorption cross section of C_2H_2 measured at ambient temperature by Cooper et al. (1995). In the first simulation, we used the C_2H_2 absorption cross sections obtained at LISA at ambient temperature for the spectral range of 115–228 nm, whereas in the second simulation, we employed high temperature absorption cross sections measured at 773 K. For wavelengths longer than 228 nm, we assumed zero absorption for C_2H_2 . We did not change the absorption cross sections of the other molecules between the simulations. To reduce the computational time, the model used a resolution of 1 nm for both the stellar flux and the absorption cross sections. Our data have thus been reduced to this resolution. At longer wavelengths, Bénilan et al. (2000) studied the dependence of the photo-dissociation rate of C_2H_2 on the spectral resolution of its absorption cross sections within the 185–235 nm spectral range. They demonstrated that, while the calculated photo-dissociation rate of C_2H_2 varies with the spectral resolution, this variation is very minor, within less than 1%. Accordingly, the high resolution does not introduce significant uncertainties into the resulting values calculated by the model.

3.3.5. Photodissociation rate of C_2H_2

To quantify the effect of the change of the absorption cross section with the temperature on the photo-dissociation and subsequently on the modeled molecular abundances, we can compare the photodissociation rate (s^{-1}) of C_2H_2 in our two different simulations described above. In our model, following the assumption of Hébrard et al. (2013); Heays et al. (2017); Vuitton et al. (2019) based on the quantum yield measurements of Läuter et al. (2002), we consider only one C_2H_2 photodissociation route:



with a quantum yield of one from 120 to 217 nm. From 72 to 120 nm, we used the quantum yield recommended by Huebner & Mukherjee (2015).

Figure 9 presents the photodissociation rate of C_2H_2 as a function of pressure in our two simulations. For pressures lower than 10^{-2} bar, we emphasize that the photodissociation rate of C_2H_2 is three times higher when using the absorption cross section at 773 K. This increase in the photodissociation rate in the upper atmosphere is attributed to the rise in the absorption cross section with temperature. In addition, we observed that when using $\sigma_{C_2H_2}$ (773 K), the photodissociation rate becomes negligible below $P \sim 5 \times 10^{-1}$ bar, indicating that no photodissociation of C_2H_2 occurs at deeper atmospheric levels. However, when using $\sigma_{C_2H_2}$ (296 K), C_2H_2 photodissociation occurs down to $\sim 2 \times 10^{-1}$ bar. This can be explained by a change in the penetration of the actinic flux into the atmosphere, depending on the

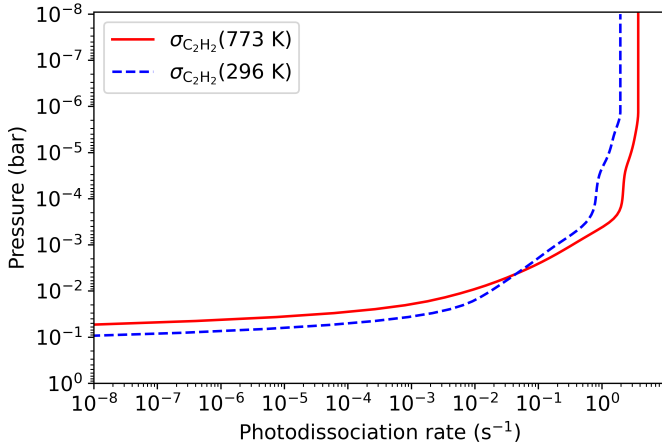


Fig. 9. Photodissociation rates of C_2H_2 in our atmospheric model using the absorption cross section of C_2H_2 measured at 296 K (dashed blue line) and 773 K (full red line).

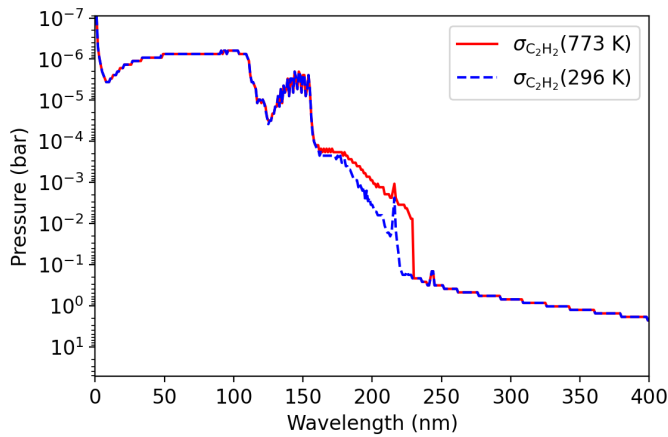


Fig. 10. Penetration of the actinic flux in the atmosphere (level where the optical depth is equal to 1) when using $\sigma_{C_2H_2}$ (296 K) (dashed blue line) and $\sigma_{C_2H_2}$ (773 K) (full red line). This takes into account absorption and diffusion by the different chemical species presents in the atmosphere.

absorption cross section of acetylene used. Figure 10 presents, for our two simulations, the altitude at which the optical depth of atmosphere reaches a value of one as a function of wavelength, considering the absorption and diffusion processes by various chemical species present in the atmosphere. In the spectral range of 150–228 nm, where the absorption is primarily dominated by C_2H_2 , we observe that the actinic flux penetrates less deeply in the atmosphere when using data at 773 K. This is consequently due to the increases in the absorption cross section of C_2H_2 at higher temperature. It should be noted that the discontinuity observed at 228 nm in the simulation using $\sigma_{C_2H_2}$ (773 K) arises from assumption of zero absorption by acetylene at longer wavelengths. Therefore, the opacity of the atmosphere calculated by the model passes abruptly from a domain governed by C_2H_2 absorption to one potentially dominated by Rayleigh diffusion. Even if not observed in this study, such an impact on the penetration of the stellar flux could have significant consequences for the abundance of other absorbing species, resulting in lower degree of photodissociation, and thus higher abundances. For instance, the self-shielding mechanism could explain isotopic ratios anomalies in planetary atmospheres due to the isotope fractionation (Chakraborty et al. 2014; Lyons 2020;

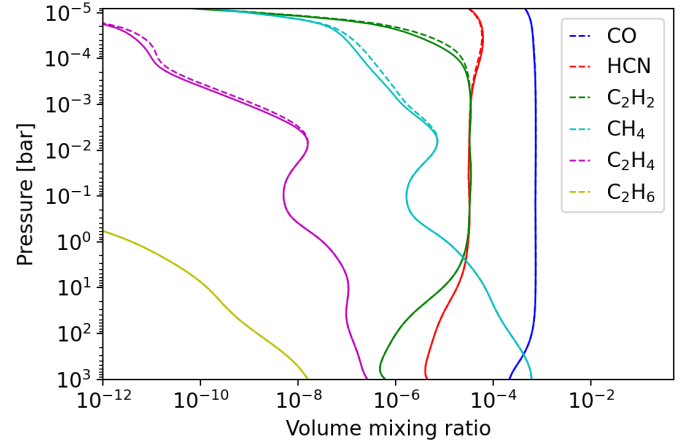


Fig. 11. Abundance profiles for the main hydrocarbons at steady state in the atmosphere of our hypothetical planet. Solid lines correspond to the abundances calculated using the absorption cross section of C_2H_2 measured at 773 K, and dotted lines correspond to 296 K.

Lyons & Young 2005). While we did not specifically attempt to investigate this mechanism of shielding, such an effect was observed with CO_2 in a similar study (Venot et al. 2018) when analyzing chemical pathways.

3.3.6. Composition at the steady state

Figure 11 presents the vertical volume mixing ratio profiles for the main hydrocarbons, as well as CO, at steady state for the two simulations. After dihydrogen (H_2) and helium (He), which are not shown in the figure, the atmosphere is dominated by CO ($\sim 10^{-3}$), hydrogen cyanide (HCN), C_2H_2 , and CH_4 . This is a consequence of the high C/O ratio chosen for our simulations. A solar C/O ratio would have led to an amount of H_2O almost similar to that of CO, and a very low abundance of hydrocarbons (Venot et al. 2015). In our simulations, the other C_2 hydrocarbons, that is ethylene (C_2H_4) and ethane (C_2H_6), are less important and have volume mixing ratios lower than 10^{-6} .

We observe in Fig. 11 that the abundance profile of C_2H_2 is slightly modified in the high atmosphere when the absorption cross section measured at 773 K is used instead of the one at 296 K, with a decrease of 40% around 5×10^{-5} bar. This finding is similar to that obtained for CO_2 by Venot et al. (2018). Indeed, they observed that the change in CO_2 abundance was not significant even though the absorption cross section of CO_2 increases by four orders of magnitude in the longer wavelength spectral domain at 773 K compared to 296 K. In Fig. 11, we note also that other species undergo variations in abundance, such as HCN, which becomes slightly more abundant when using $\sigma_{C_2H_2}$ at 773 K and most notably CH_4 and C_2H_4 , where their abundances diminished down to 10^{-2} bar, showing the strong coupling between molecules through chemical reactions.

4. Conclusions

We have measured experimentally for the first time the thermal dependence of the VUV absorption cross section of C_2H_2 at seven temperatures ranging from 296 to 793 K and over a large spectral range extending from 115 to 230 nm.

We found that the absolute absorption cross section of C_2H_2 increases with temperature. We observed an increase in the intensity of the continuum and a decrease in the intensity of the

absorption bands as the gas temperature increase, which result in an overall increase in the absolute absorption cross section of C₂H₂ with temperature. From 116 to 185 nm, the continuum increases is relatively constant across the whole wavelengths range at a given temperature (e.g., a F_T of 0.5 at 773 K), while the variations in certain bands can be more important (up to a F_T of 3.5 at 773 K). Beyond 185 nm, the increase is more important and reaches a maximum of a factor of 20 around 220 nm, which agrees with the presence of numerous hot bands in this region. In addition to these general variations, we observe at 473 K (and at higher temperatures) a new absorption band at ~156.7 nm, whose intensity increases together with the temperature. We identify it as a hot band, which originates from the vibrational mode ν_2 ($\nu_2 = 1973.8 \text{ cm}^{-1}$).

To go further, we quantified the impact of these new data on the prediction of exoplanet atmospheres composition using the 1D thermo-photochemical model FRECKLL. After modeling a hypothetical exoplanet atmosphere, we found that the abundance profile of C₂H₂ is slightly changed when the absorption cross section of C₂H₂ measured at 773 K is used instead of the one at 296 K, with a decrease of 40% around 5×10^{-5} bar. In addition, these changes in the absorption cross sections of C₂H₂ affect the penetration of the actinic flux through the atmosphere from 150 to 230 nm, resulting in an attenuation of the flux at higher altitudes when using the cross section measured at 773 K compared to the ones measured at 296 K. Although we did not compute it, we do not expect this slight change of the C₂H₂ abundance profile to have a visible impact on the synthetic spectrum of the simulated atmosphere, and to thus be visible in observational data.

Finally, the present study only investigates the effect of the thermal dependence of the absorption cross section of C₂H₂ on simulated atmospheric compositions. However, similar changes in the absorption cross section with temperature have been observed for CO₂ (Venot et al. 2013, 2018) and can be expected for numerous species present in exoplanet atmospheres. It is therefore essential to measure the thermal dependence of the VUV absorption cross section of all major species observed in exoplanet atmospheres, knowing that the effect of photochemistry on the composition of an exoplanet atmosphere has now been observed with JWST (Tsai et al. 2023; Dyrek et al. 2024).

Acknowledgements. This work is supported by the ANR project ‘EXACT’ (ANR-21-CE49-0008-01), the Centre National d’Etudes Spatiales (CNES), and the CNRS/INSU Programme National de Planétologie (PNP). B.F. thanks the Université Paris-Est Créteil (UPEC) for funding support (postdoctoral grant).

References

- Aghsaee, M., Dürrstein, S. H., Herzler, J., et al. 2014, *Combust. Flame*, **161**, 2263
- Alderson, L., Wakeford, H. R., Alam, M. K., et al. 2023, *Nature*, **614**, 664
- Al-Refai, A. F., Venot, O., Changeat, Q., & Edwards, B. 2024, *ApJ*, **967**, 132
- Baeyens, R., Konings, T., Venot, O., Carone, L., & Decin, L. 2022, *MNRAS*, **512**, 4877
- Benson, S. W. 1992, *Int. J. Chem. Kinet.*, **24**, 217
- Boyé, S., Campos, A., Fillion, J.-H., et al. 2004, *Comptes Rend. Phys.*, **5**, 239
- Bénilan, Y., Andrieux, D., & Bruston, P. 1995, *Geophys. Res. Lett.*, **22**, 897
- Bénilan, Y., Smith, N., Jolly, A., & Raulin, F. 2000, *Planet. Space Sci.*, **48**, 463
- Chakraborty, S., Muskatel, B. H., Jackson, T. L., et al. 2014, *Proc. Natl. Acad. Sci. U.S.A.*, **111**, 14704
- Chen, F. Z., & Wu, C. Y. R. 2004, *JQSRT*, **85**, 195
- Chen, F., Judge, D. L., Robert Wu, C. Y., et al. 1991, *J. Geophys. Res.: Planets*, **96**, 17519
- Cheng, B.-M., Lu, H.-C., Chen, H.-K., et al. 2006, *ApJ*, **647**, 1535
- Cheng, B.-M., Chen, H.-F., Lu, H.-C., et al. 2011, *ApJS*, **196**, 3
- Chubb, K. L., Robert, S., Sousa-Silva, C., et al. 2024, *RAS Techniques and Instruments*, **3**, 636
- Colket, M. B., Seery, D. J., & Palmer, H. B. 1989, *Combust. Flame*, **75**, 343
- Cooper, G., Burton, G. R., & Brion, C. E. 1995, *J. Electron Spectrosc. Related Phenom.*, **73**, 139
- Cridland, A. J., van Dishoeck, E. F., Alessi, M., & Pudritz, R. E. 2019, *A&A*, **632**, A63
- de Oliveira, N., Roudjane, M., Joyeux, D., et al. 2011, *Nat. Photon.*, **5**, 149
- Drummond, B., Carter, A. L., Hébrard, E., et al. 2019, *MNRAS*, **486**, 1123
- Duran, R. P., Amorebieta, V. T., & Colussi, A. J. 1988, *J. Phys. Chem.*, **92**, 636
- Dyrek, A., Min, M., Decin, L., et al. 2024, *Nature*, **625**, 51
- Es-sebbar, E., & Farooq, A. 2014, *JQSRT*, **149**, 241
- Foo, P. D., & Innes, K. K. 1973, *Chem. Phys. Lett.*, **22**, 439
- Fortney, J., Robinson, T. D., Domagal-Goldman, S., et al. 2019, *Astro2020: Decadal Survey on Astronomy and Astrophysics*, 2020, 146
- Gedanken, A., & Schnepf, O. 1976, *Chem. Phys. Lett.*, **37**, 373
- Giacobbe, P., Brogi, M., Gandhi, S., et al. 2021, *Nature*, **592**, 205
- Grosch, H., Fateev, A., & Clausen, S. 2015, *JQSRT*, **154**, 28
- Guzmán-Mesa, A., Kitzmann, D., Mordasini, C., & Heng, K. 2022, *MNRAS*, **513**, 4015
- Heays, A. N., Bosman, A. D., & van Dishoeck, E. F. 2017, *A&A*, **602**, A105
- Herbert, F., Sandel, B. R., Yelle, R. V., et al. 1987, *J. Geophys. Res.: Space Phys.*, **92**, 15093
- Herzberg, G. 1966, *Molecular Spectra and Molecular Structure*. 3: Electronic Spectra and Electronic Structure of Polyatomic Molecules
- Hu, R., Seager, S., & Yung, Y. L. 2015, *ApJ*, **807**, 8
- Huebner, W. F., & Mukherjee, J. 2015, *Planet. Space Sci.*, **106**, 11
- Hébrard, E., Dobrijevic, M., Loison, J. C., et al. 2013, *A&A*, **552**, A132
- Hörst, S. M. 2017, *J. Geophys. Res.: Planets*, **122**, 432
- Kawashima, Y., & Masahiro, I. 2018, *ApJ*, **853**, 7
- Kern, R. D., Xie, K., Chen, H., & Kiefer, J. H. 1991, *Symp. (Int.) Combust.*, **23**, 69
- Läuter, A., Lee, K. S., Jung, K. H., et al. 2002, *Chem. Phys. Lett.*, **358**, 314
- Line, M. R., Liang, M. C., & Yung, Y. L. 2010, *ApJ*, **717**, 496
- Line, M. R., Gautam, V., Pin, C. D., A., & Yuk L., Y. 2011, *ApJ*, **738**, 32
- Liu, M., Chu, T.-C., Jocher, A., et al. 2021, *Int. J. Chem. Kinet.*, **53**, 27
- Lodders, K. 2010, in *Principles and Perspectives in Cosmochemistry*, eds. A. Goswami, & B. E. Reddy (Springer Berlin Heidelberg), 379
- Lyons, J. 2020, *Geochim. Cosmochim. Acta*, **282**, 177
- Lyons, J. R., & Young, E. D. 2005, *Nature*, **435**, 317
- Macy, W. 1980, *Icarus*, **41**, 153
- Madhusudhan, N. 2012, *ApJ*, **758**, 36
- Madhusudhan, N., Mousis, O., Johnson, T. V., & Lunine, J. I. 2011, *ApJ*, **743**, 191
- Meyn, L. 2000, *An Uncertainty Propagation Methodology that Simplifies Uncertainty Analyses* (American Institute of Aeronautics & Astronautics)
- Moos, H. W., & Clarke, J. T. 1979, *ApJ*, **229**, L107
- Moses, J. I. 2014, *Philos. Trans. A Math. Phys. Eng. Sci.*, **372**, 20130073
- Moses, J. I., Visscher, C., Fortney, J. J., et al. 2011, *ApJ*, **737**
- Moses, J. I., Line, M. R., Visscher, C., et al. 2013a, *ApJ*, **777**, 34
- Moses, J. I., Madhusudhan, N., Visscher, C., & Freedman, R. S. 2013b, *ApJ*, **763**, 25
- Nahon, L., de Oliveira, N., Garcia, G. A., et al. 2012, *J. Synchrotron Radiat.*, **19**, 508
- Nakayama, T., & Watanabe, K. 1964, *J. Chem. Phys.*, **40**, 558
- Nixon, C. A. 2024, *ACS Earth Space Chem.*, **8**, 406
- Nobre, M., Fernandes, A., Ferreira da Silva, F., et al. 2008, *Phys. Chem. Chem. Phys.*, **10**, 550
- Orton, G. S., Aitken, D. K., Smith, C., et al. 1987, *Icarus*, **70**, 1
- Parmentier, V., & Guillot, T. 2014, *A&A*, **562**, A133
- Poveda, M. 2023, Ph.D. Thesis, Université Paris Est, France
- Powell, D., Feinstein, A. D., Lee, E. K. H., et al. 2024, *Nature*, **626**, 979
- Ranjan, S., Schwieterman, E. W., Harman, C., et al. 2020, *ApJ*, **896**, 148
- Ridgway, S. T. 1974, *ApJ*, **187**, L41
- Rocchetto, M., Waldmann, I. P., Venot, O., Lagage, P. O., & Tinetti, G. 2016, *ApJ*, **833**, 120
- Rufus, J., Stark, G., Thorne, A. P., et al. 2009, *J. Geophys. Res.: Planets*, **114**
- Segura, A., Krellove, K., Kasting, J. F., et al. 2003, *Astrobiology*, **3**, 689
- Smith, P. L., Yoshino, K., Parkinson, W. H., Ito, K., & Stark, G. 1991, *J. Geophys. Res.: Planets*, **96**, 17529
- Stern, S. A., Bagenal, F., Ennico, K., et al. 2015, *Science*, **350**, aad1815
- Suto, M., & Lee, L. C. 1984, *J. Chem. Phys.*, **80**, 4824
- Tennyson, J., Yurchenko, S. N., Zhang, J., et al. 2024, *JQSRT*, **326**, 109083
- Thuillier, G., Floyd, L., Woods, T. N., et al. 2004, *Solar Irradiance Reference Spectra* (American Geophysical Union (AGU)), 171
- Tsai, S.-M., Malik, M., Kitzmann, D., et al. 2021, *ApJ*, **923**, 264
- Tsai, S.-M., Lee, E. K. H., Powell, D., et al. 2023, *Nature*, **617**, 483

- Van Craen, J. C., Herman, M., Colin, R., & Watson, J. K. G. 1985, *J. Mol. Spectrosc.*, **111**, 185
- Van Craen, J. C., Herman, M., Colin, R., & Watson, J. K. G. 1986, *J. Mol. Spectrosc.*, **119**, 137
- Vattulainen, J., Wallenius, L., Stenberg, J., Hernberg, R., & Linna, V. 1997, *Appl. Spectrosc.*, **51**, 1311
- Veillet, R., Venot, O., Sirjean, B., et al. 2024, *A&A*, **682**, A52
- Venot, O., Fray, N., Bénilan, Y., et al. 2013, *A&A*, **551**, A131
- Venot, O., Hébrard, E., Agúndez, M., Decin, L., & Bounaceur, R. 2015, *A&A*, **577**, A33
- Venot, O., Bénilan, Y., Fray, N., et al. 2018, *A&A*, **609**, A34
- Venot, O., Parmentier, V., Blecic, J., et al. 2020, *ApJ*, **890**
- Vuitton, V., Yelle, R. V., Klippenstein, S. J., Hörst, S. M., & Lavvas, P. 2019, *Icarus*, **324**, 120
- Watson, J. K. G., Herman, M., Van Craen, J. C., & Colin, R. 1982, *J. Mol. Spectrosc.*, **95**, 101
- Weng, W., Li, S., Aldén, M., & Li, Z. 2021, *Appl. Spectrosc.*, **75**, 1168
- Wu, C. Y. R., Chien, T. S., Liu, G. S., Judge, D. L., & Caldwell, J. J. 1989, *J. Chem. Phys.*, **91**, 272
- Wu, R. C. Y., Yang, B. W., Chen, F. Z., et al. 2000, *Icarus*, **145**, 289
- Wu, C. Y. R., Chen, F. Z., & Judge, D. L. 2001, *J. Geophys. Res.: Planets*, **106**, 7629
- Wu, C. Y. R., Chen, F. Z., & Judge, D. L. 2004, *J. Geophys. Res.: Planets*, **109**
- Wu, Y.-J., Lu, H.-C., Chen, H.-K., et al. 2007, *J. Chem. Phys.*, **127**, 154311
- Zabeti, S., Fikri, M., & Schulz, C. 2017, *Proc. Combust. Inst.*, **36**, 4469
- Zádor, J., Fellows, M. D., & Miller, J. A. 2017, *J. Phys. Chem. A*, **121**, 4203